Modelling colloid adsorption in porous media

A qualitative and quantitative analysis

June 2018

Frederik Bokma

5573815

Master thesis Earth surface and water

Supervisor: dr. Amir Raoof

Second supervisor: prof. dr. Ruud Schotting

Utrecht University

Abstract

Accurate knowledge of the processes that control the transport and deposition of colloids in subsurface environments is needed to protect water resources from a wide variety of contaminants. Applied hydrodynamics can play a significant role in colloid retention but is not yet fully understood.

In this thesis, the effect of pore shape and velocity on colloid attachment and detachment is researched by performing single pore simulations in MATLAB. The model is based on the geometry of a parabolic constricted tube and simulates a fluid flow through this pore.

Firstly, the model was run with only two changed parameters: the constriction radius and the velocity through the chokepoint (μ). The speed is changed from low (0.3e-6 m/s) to average (1.5e-6 m/s) to high (3e-6 m/s). Each speed is run with three constriction radii: small (0.02e-3 m), average (0.15e-3 m) and straight (0.3e-3 m). The results from the 9 (3x3) model runs are grouped and plotted together for colloid attachment vs constriction radius and colloid attachment vs velocity. Secondly, a comparison is made between increasing velocities (3e-6 m/s, 6e-6 m/s, 12e-6 m, 30e-6 m/s, 60e-6m/s and 120e-6 m/s) and colloid retention.

I conclude that colloid attachment and detachment is indeed affected by pore shape geometry and applied hydrodynamics. The effects are strongest at the extremes: no adsorption in straight pores and high adsorption in narrow pores. During average constriction radii the effect is the lowest.

Further research (based on the model and conclusions of this study) increases our understanding and have a potentially substantial impact on a wide spectrum of subjects, from medicine to water treatment.

Contents

1. Introduction

Many water treatment techniques depend on granular filtration to cleanse the water. Granular filtration is a mechanism wherein water flows through a granular material while suspended solids are retained inside the medium. The retained substances can be biochemically decomposed and pathogenic microorganisms (e.g. bacteria, viruses and protozoa) removed, (TU Delft, n.d.). The size of the suspended solids can vary from nano to the mm scale. The small suspended solids carry the term colloids. A colloid is a substance which consists of particles which have at least one dimension in the size range from 1 to 1000 nm, e.g. dust (Brittanica Online Encyclopedia, n.d.).

Accurate knowledge of the processes that control the transport and deposition of colloids in subsurface environments is needed to protect water resources from a wide variety of contaminants. The importance of adhesive and diffusion forces on colloid retention is well established, and theory has been developed in order to predict these factors (Tufenkji & Elimelech, 2005). Conversely, the role of hydrodynamic forces on colloid retention has received considerably less attention. Previous research has indicated that the applied hydrodynamics can play a significant role in colloid retention in several natural environments (Torkzaban, Bradford, & Walker, 2007).

In this study, the effect of applied hydrodynamics on the colloid transport will be studied. In addition to hydrodynamic and drag force, other forces applied on colloid such as gravity, London-van der Waals, Double-Layer, Brownian motion will also be included. First, single pore simulations will be performed to model movement of colloids and to calculate forces for different pores depending on the geometry of the pore as well as the colloid size. This way relations for colloid attachment and detachment in a single pore based on the pore shape and other factors such as water velocity can be calculated. Using this method colloid transport can be simulated in various soils with different pore-size distributions as well as different topological properties, such as pore connectivities.

The aim of this study is to research what the effect of applied hydrodynamics is on the colloid retention in a porous medium. To do this a single pore will be modelled in MATLAB. The model will be based on the geometry of a parabolic constricted tube. The model will simulate a fluid flow through this pore with a number of colloids starting at the top, and it will run until all the colloids have been adsorbed or passed through the pore.

This will allow for a precise way to regulate both fluid flow and pore geometry, to accurately assess the effect of the applied hydrodynamics on pore colloid retention. The velocity field calculations for the model were, in part, drawn from Chang et al. (2003).

The main research questions is:
"How is colloid attachment and detachment in a single pore affected by pore shape and velocity?"

This thesis is organised in the following way. It begins by laying out the theoretical framework of the research (2). The section thereafter describes the methodology (3), followed by the results (4), the discussion and a presentation of the concluding remarks (5).

2. Theoretical Framework

This chapter gives a theoretical background by answering the following questions:

- How to model waterflow in porous media? (2.1)
- What is known about colloid retention already? (2.2)
- What is the role of hydrodynamics? (2.3)
- What formulas are used? (2.4)

2.1 How to model waterflow in porous media?

One of the first to establish a conceptual model of a granular medium were Payatakes et al. (1973) and Tien and Payatakes (1979) (Tien & Ramarao, 2007). They represented a homogenous, randomly packed medium as consisting of a number of unit bed elements (UBE) in series (Fig. 1). A UBE consists of an amount of collectors, which can be presented in a number of ways: the capillaric model, spherical model and the constricted-tube model.

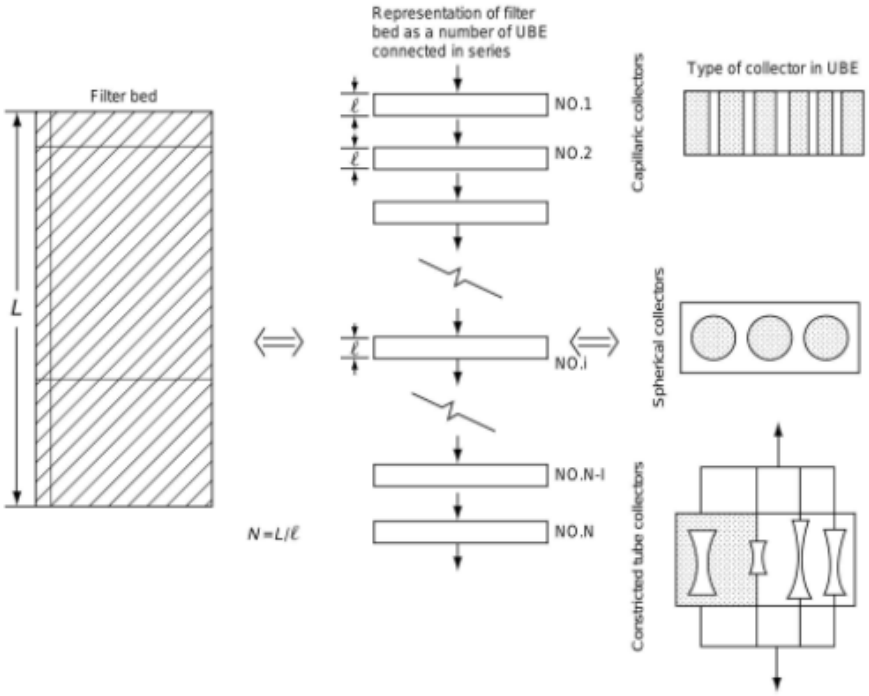

Figure 1. This figure represents a way of describing the filter bed as a series of UBE's, which can possibly have different collector geometries. Source: (Tien & Ramarao, 2007)..

The capillary model

The capillary model represents a granular medium as a collection of straight capillaries of similar size. This is one of the oldest and simplest porous media models (Tien & Ramarao, 2007). Since Darcy's law governs flow through porous media and flow through the capillaries can be described by Hagen-Poiseuille, these

formulas can be combined into a set of equations which require only macroscopic properties of the medium to solve the properties of filter bed. The properties are average grain diameter, bed porosity and permeability (Tien & Ramarao, 2007).

The spherical model

In a lot of cases a granule of a granular medium can be viewed as a sphere, thereby the whole of the granular medium can viewed as a collection of spheres which act as collectors (Tien & Ramarao, 2007). The flow field can be readily be described by the stream function. Further subdivision can be made within the spherical model group but are not important to the focus of this thesis and are therefore not mentioned in detail.

The constricted tube model

The constricted tube model assumes that the voids within a granular medium are pore spaces connected by constrictions. A description of the constricted tube model was first provided by Payatakes et al. (1973). They described voids of porous media as "a collection of pore spaces connected by constrictions such that the basic flow channel through the media is assumed to consist of two half pores joined by a constriction and aligned along the direction of the main flow" (Tien & Ramarao, 2007).

In a UBE, the constricted tube shape and sizes can vary. The characterising dimensions of each constricted tube are constriction diameter, maximum diameter and height.

The walls of the tube can be constricted in three different ways: parabolic, sinusoidal and hyperbolic (Fig. 2).

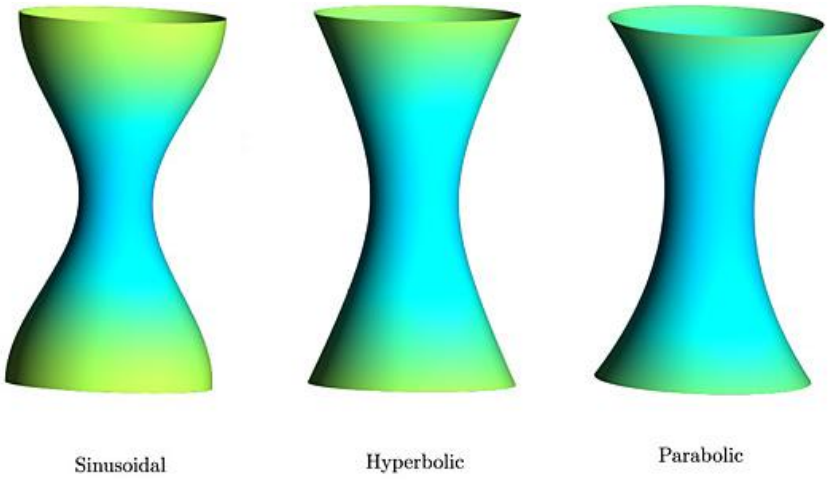

Figure 2. This picture shows the different tube shapes: sinusoidal, hyperbolic and parabolic. Source: (Sochi, 2013).

The flowfield within a constricted tube is axisymmetrical and two-dimensional, first convergent then divergent. Chow and Soda developed a general solution for the flowfield in 1972. They considered the wall radius as an arbitrary function of the axial distance, instead of any specific geometry. This was later modified by Chang & Tien (1985a) and used with parabolic constricted tube geometry in this thesis. All models merely approximate granular media, which is highly complex and chaotic, and do so by way of a highly simplified picture.

2.2 What is known about colloid retention already?

There are a number of different forces involved in the retention of colloids: molecular dispersion, electrokinetic and hydrodynamics forces. In this thesis the model accounts for drag (hydrodynamics), gravity, Brownian motion (i.e. dispersion) and DLVO-forces (electrokinetic).

The DLVO-theory is named after Boris **D**erjaguin, Lev **L**andau, Evert **V**erwey and Theodoor **O**verbeek. This theory describes the force between charged surfaces interacting through a liquid medium. When two particles or a particle and a surface approach each other, their ionic atmospheres begin to overlap and a repulsion force is developed (Zeta-Meter, 1997). But at the same time the Van der Waals attraction force increases with decreasing distance, just as the repulsion force.

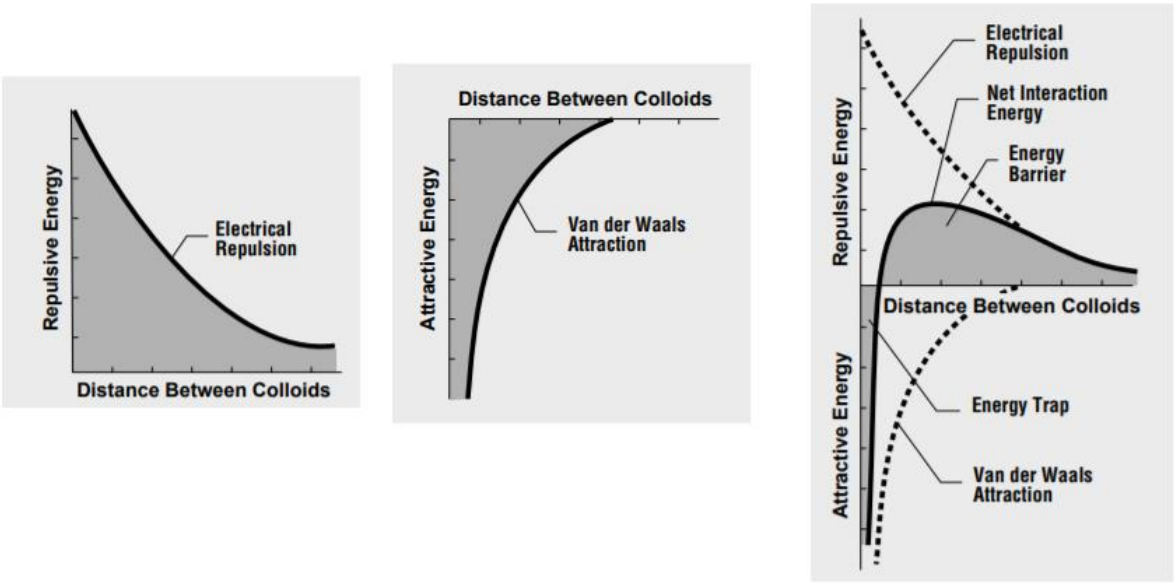

Figure 3. These figures depict a schematic of the energy barrier and the forces out of which it is constructed. Source: (Zeta-Meter, 1997).

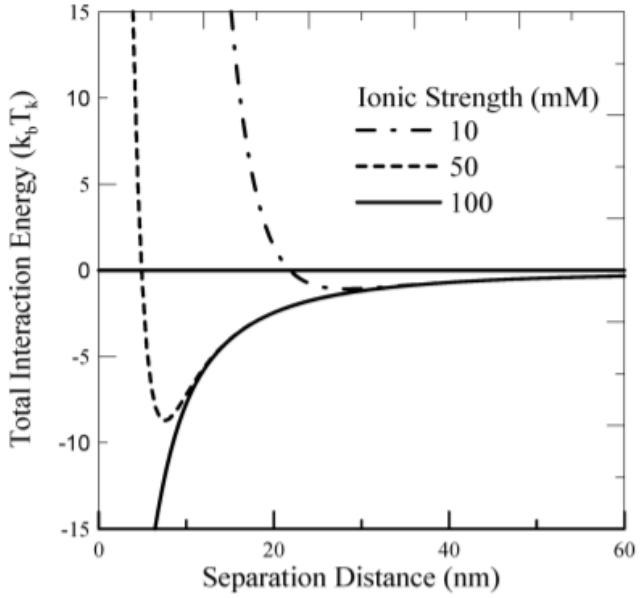

Figure 4. This figure shows the total interaction energy as a function of separation distance between different colloids at several ionic strengths. Source: (Torkzaban et al., 2007).

This creates an energy barrier for colloids to overcome before they can aggregate (Fig. 3). If the energy barrier is overcome the colloids can successfully aggregate, and are stuck in an energy trap, called the primary minimum. In the primary minimum, the particles are forced to aggregate which is irreversible (Boström, Deniz, Franks, & Ninham, 2006). If the energy barrier is too high to overcome, colloidal particles may stay in the secondary energy minimum, where they are held together by weaker bonds. Colloidal particles at the secondary energy minimum can be dispersed back into the solution or flow along the surface due to hydrodynamic forces. The third option is that the colloid cannot overcome the energy barrier and rebounds back, resulting in no aggregation at all. Different ionic strengths can result in different energy curves (Fig. 4), leading to weaker or stronger energy barriers, which affects aggregation.

2.3 What is the role of hydrodynamics?

Colloid filtration theory (CFT) developed by Yao et al. (1971) explains colloid deposition under saturated conditions and is commonly used to describe filtration (Torkzaban et al., 2007). This theory explains deposition in terms of single collector efficiency (n) and collision efficiency (a). The variable (n) governs the mass flow, it is "the rate at which particles strike the collector divided by the rate of particles which flow toward the collector" (Yao, Habibian, & O'Melia, 1971).

2.4 What formulas are used?

Flow field

Equations for the flow field were established by Chow and Soda (1972), later modified by Chiang & Tien (1985) and summarised by Chang et al. (2003). This equation assumes the wall radius as an arbitrary function of the axial distance in a constricted tube (Chang, Chen, & Lee, 2003).

Equations:

$$\psi^* = \frac{\psi}{u_m r_m^2} = \psi_0^* + R_m \psi_1^* + R_m^2 \psi_2^*$$

The zero, first and second order solutions of the stream function are given down below (1, 2, 3).

1

$$\psi_0^* = 0.5(R^4 - 2R^2)$$

2

$$\psi_1^* = 0.25 N_{Re,m} \frac{dR_w/dZ}{R_w} \left[\frac{1}{9}(R^8 - 6R^6 + 9R^4 - 4R^2)\right]$$

3

$$\psi_2^* = -0.5\left[5\left(\frac{dR_w}{dZ}\right)^2 - R_w \frac{d^2R_w}{dZ^2}\right]\frac{(R^2-1)R^2}{3} - 0.125 N_{Re,m}\left(\frac{dR_w/dZ}{R_w}\right)^2 [32R^{12} - 305R^{10} + 750R^8 - 713R^6 + 236R^4]/3600$$

Where

1.1

$$Z = \frac{z}{l_f}$$

In this formula the distance z is divided by the total distance lf, resulting in the dimensionless tube length Z.

1.2

$$R_w = \frac{r_w}{r_m}$$

1.3

$$R = \frac{r}{r_w}$$

In this formula the dimensionless distance to the wall of the pore, R is created. This is done by dividing distance to the pore wall by total length.

1.4

$$R_m = \frac{r_m}{l_f}$$

1.5

$$r_m = \frac{1}{l_f}\int_0^{l_f} r_w dz$$

In this formula the average distance to the wall throughout the entire pore is calculated, rm. This is done by calculating the surface area of the pore and dividing it by total pore length lf.

1.6

$$N_{Re,m} = \frac{u_m r_m \rho_f}{\mu}$$

The formula (1.6) is for calculating the Reynolds number. Um is average speed through the pore constriction, rm is average distance to the pore wall, pf is fluid density and mu is dynamic viscosity,

1.7

$$u_s = (u_m)(\pi r_m^2)N_c$$

1.8

$$u_r = u_m(u_{r0}^* + R_m u_{r1}^* + R_m^2 u_{r2}^*)\frac{r_m^2}{r_w l_f}$$

This formula is for calculating the r-direction component of the velocity in a specific location.

1.9

$$u_z = u_m(u_{z0}^* + R_m u_{z1}^* + R_m^2 u_{z2}^*)\frac{r_m^2}{r_w^2}$$

This formula is for calculating the z-direction component of the velocity in a specific location.

2.0

$$u_{r0}^* = -2\frac{dR_w/dZ}{R_w}(R^3 - R)$$

2.1

$$u_{r1}^* = \frac{0.25}{R}N_{Re,m}\left\{F\left[\frac{d^2R_w/dZ^2}{R_w} - \left(\frac{dR_w/dZ}{R_w}\right)^2\right] + \frac{dF}{dZ}\frac{dR_w/dZ}{R_w}\right\}$$

2.2

$$u_{r2}^{*} = -0.5\left\{\left(9\frac{dR_w}{dZ}\frac{d^2R_w}{dZ^2} - R_w\frac{d^3R_w}{dZ^3}\right)\frac{G}{R} + \left[5\left(\frac{dR_w}{dZ}\right)^2 - R_w\frac{d^2R_w}{dZ^2}\right]\frac{dG}{RdZ}\right\}$$
$$- 0.125\left\{2\frac{dR_w/dZ}{R_w}\left[\frac{d^2R_w/dZ^2}{R_w} - \left(\frac{dR_w/dZ}{R_w}\right)^2\right]\frac{E}{R} + \left(\frac{dR_w/dZ}{R_w}\right)^2\frac{dE}{RdZ}\right\}$$

2.3

$$u_{z0}^{*} = 2(1 - R^2)$$

2.4

$$u_{z1}^{*} = -\frac{0.25}{R}N_{Re,m}\frac{dF}{dR}\frac{dR_w/dZ}{R_w}$$

2.5

$$u_{z2}^{*} = 0.5\left[5\left(\frac{dR_w}{dZ}\right)^2 - R_w\frac{d^2R_w}{dZ^2}\right]\frac{dG}{RdR} + 0.125N_{Re,m}\left(\frac{dR_w/dZ}{R_w}\right)^2\frac{dE}{RdZ}$$

2.6

$$F = (R^8 - 6R^6 + 9R^4 - 4R^2)/9$$

2.7

$$G(R^2 - 1)R^2/3$$

2.8

$$E = (32R^{12} + 305R^{10} + 750R^8 - 713R^6 + 236R^4)/3600$$

The equations given above are used for solving the stream function. Solving these equations would result in a flow line chart as seen in figure 5 and 6.

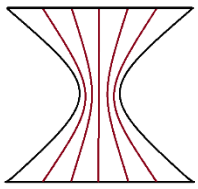

Figure 5. Simple depiction of streamlines in a constricted tube.

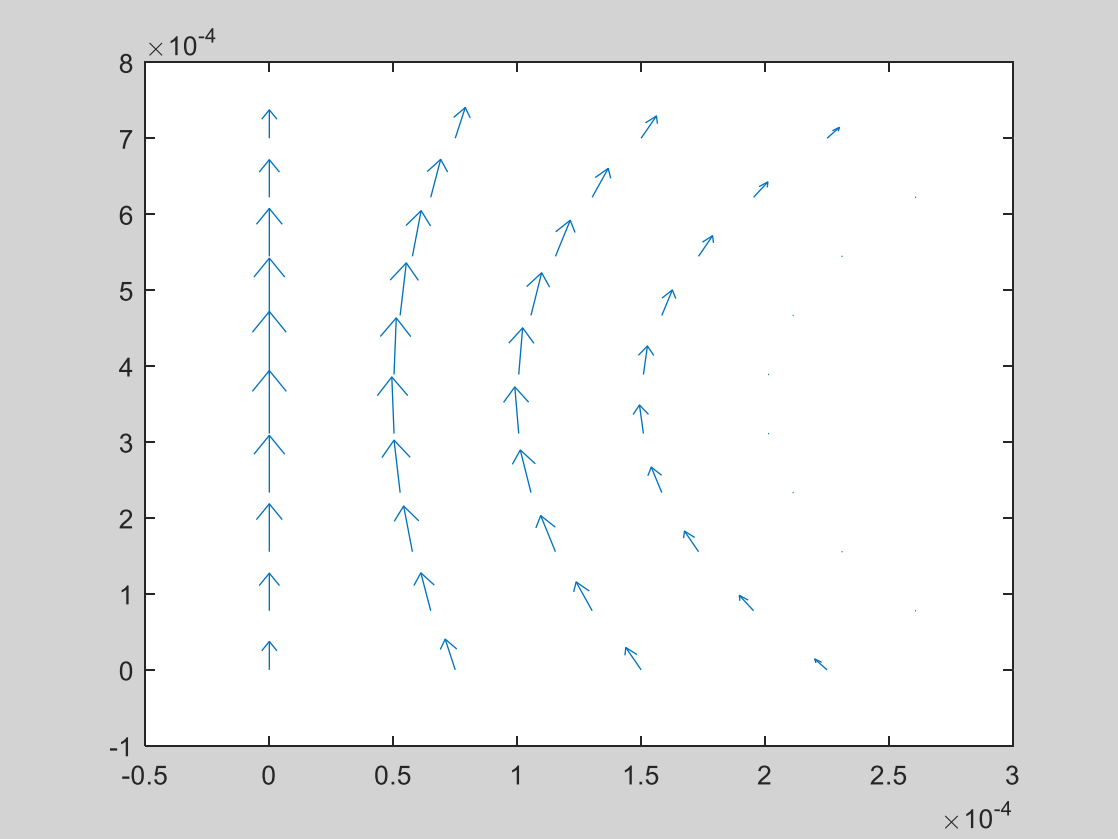

Figure 6. This figure shows the velocity field in one half of a constricted tube. The numbers displayed are in meters [m].

Model framework

This section will give information about the underlying theory and literature upon which the model is based, most of which comes from unpublished work of dr. Amir Raoof. We start with a formula like the first law of newton, where mass times acceleration equals the summation of all forces.

Without Brownian motion, the deterministic trajectory equation will be:

(29)

$$m_p \frac{d\bar{U}}{dt} = -f(\eta, n_f)\left(\bar{\bar{K}}_t . \bar{U} + \bar{\bar{K}}_c^T . \bar{\Omega}\right) + \bar{F}$$

$$I_n \frac{d\bar{U}}{dt} = -f(\eta, n_f)\left(\bar{\bar{K}}_r . \bar{\Omega} + \bar{\bar{K}}_c . \bar{\mathrm{U}}\right) + \bar{T}_0$$

Where Kt is related to translational velocity, Kr is related to rotational velocity and Kc is the coupling between both. F(n,nf) is a function which depends upon the viscosity of the particle and fluid, which can be simplified to f(n,nf)=n in the case of a solid particle.

If the particle inertia effects are ignored:

(30)

$$-f(\eta, n_f)\left(\bar{\bar{K}}_t.\bar{U} + \bar{\bar{K}}_c^T.\bar{\Omega}\right) = \bar{F}$$
$$-f(\eta, n_f)\left(\bar{\bar{K}}_r.\bar{\Omega} + \bar{\bar{K}}_c.\bar{\mathrm{U}}\right) = \bar{T}_0$$

We can write the above relations in matrix form and take:

(31)

$$\tilde{K} = \begin{bmatrix} \bar{\bar{K}}_t & \bar{\bar{K}}_c^T \\ \bar{\bar{K}}_r & \bar{\bar{K}}_c \end{bmatrix}$$
$$\tilde{F} = \begin{bmatrix} \bar{F} \\ \bar{T}_0 \end{bmatrix}$$

Which, when inverted, becomes:

(32)

$$\tilde{U} = \frac{1}{f(\eta, n_f)}\tilde{K}^{-1}.\tilde{F} = \tilde{M}.\tilde{F}$$

Where M denotes the ground mobility matrix which is given by:

(33)

$$\tilde{M} = \frac{1}{f(\eta, n_f)}\tilde{K}^{-1}$$

In the case of a spherical particle moving near a planar interface, eliminating the torque gives:

(34)

$$\bar{U} = \frac{d\bar{x}}{dt} = \bar{\bar{M}}.\bar{F} + \bar{\bar{M}}.\bar{\bar{K}}_c^T.\bar{\bar{K}}_r^{-1}.\bar{T}_0 = \bar{\bar{M}}.\bar{F} + \bar{\bar{M}}_c.\bar{T}_0$$

And then the expression for the mobility matrix of a solid particle near a planar interface is formulated:

(35)

$$\bar{\bar{M}} = \begin{bmatrix} M_{||} & 0 & 0 \\ 0 & M_{||} & 0 \\ 0 & 0 & M_{\perp} \end{bmatrix}$$
$$\bar{\bar{M}}_c = \begin{bmatrix} 0 & -K'_c & 0 \\ -K'_c & 0 & 0 \\ 0 & 0 & 0 \end{bmatrix} =$$

(36)

$$M_{||} = \frac{1}{6\pi\eta a} F_4'$$

$$M_{\perp} = \frac{1}{6\pi\eta a} F_1'$$

$$K_c' = \frac{1}{6\pi\eta a^2} \frac{F_6 F_4'}{F_7}$$

$$F_4' = \frac{F_4}{1 - \frac{2}{3}\frac{F_4 F_6}{F_7^2}}$$

F1, F4, F6 and F7 are the universal hydrodynamic correction functions. Since the interface is treated as a planar the correction functions (Fi) are only dependant on H, which can thus be written as Fi(H).

F1 can be well approximated for the entire range of H by using the expression:

(37)

$$F_1 = \frac{H(19H + 4)}{19H^2 + 26H + 4}$$

F4 can be interpolated for small and large separations by:

(38)

$$F_4 = \frac{1}{-\left(\frac{8}{15}\right)\ln(H) + 0.9588} \; for\; H < 0.1$$

$$F_4 = \left(\frac{H}{2.639 + H}\right)^{1/4} for\; H > 0.1$$

For large separations (H>>1) (Adamczyk, 2006; Table 3.6),

(39)

$$F_6 = \frac{1}{1 + \frac{5}{16(H+1)^3}}$$

And for distances which are closer, the expression from the Lubrication approximation is used:

(40)

$$F_6 = \frac{1}{-\left(\frac{2}{5}\right)\ln(H) + 0.3817}$$

For large separations (H>>1), F7 can be expressed as (Adamczyk, 2006; Table 3.6),

(41)

$$F_7 = 4(H+1)^2$$

And for close distances, the expression from the Lubrication approximation is used:

(42)

$$F_7 = \frac{1}{-\left(\frac{2}{15}\right)\ln(H) + 0.2526}$$

With these equations we can apply the mobility matrixes M and Mc into equation 34 and calculate the trajectory. The mobility matrixes M and Mc are only valid for solid spherical particles in the vicinity of planar interfaces. However, due to the fact that the particles are often much smaller in size than the local radius of the curvature of the interface, the interface can be treated as locally planar and thus the above matrixes can still serve as an apt approximation.

Particle trajectory

For the calculation of particle trajectory, there must be a formulation of hydrodynamic and torque forces which are acting upon the particle:

The force due to shear, which consists of components parallel to the planar surface in the x and y direction:

(43)

$$F_{sh_x} = 6\pi\eta a G_{sh_x}(P_p) F_8(z') z' \bar{\iota}_x$$

$$F_{sh_y} = 6\pi\eta a G_{sh_y}(P_p) F_8(z') z' \bar{\iota}_y$$

Z' is the particle location in the local particle coordination system, which runs normal to the planar surface of the collector. Gsh is the shear rate at the wall.

Within the hyperbolic constricted tube the flow is axisymmetric, so Gsh,y becomes 0.

The net force which acts upon a particle is the sum of the hydrodynamic forces given above and the specific Fs (e.g., van der Waals and double layer) and external Fext (e.g., electrostatic or gravitational), as well as Brownian diffusion contribution, hence:

(44)

$$F = F_h + F_s + F_{ext} + F_B$$

The hydrodynamic torque has only tangential components:

When using the method of reflections, the asymptotic expressions for F8(H) and F9(H) with large separations, can be expressed as:

(45)

$$F_8 \cong 1 + \frac{9}{16}\ \frac{1}{(H+1)}$$

$$F_9 \cong 1 - \frac{3}{16}\ \frac{1}{(H+1)^3}$$

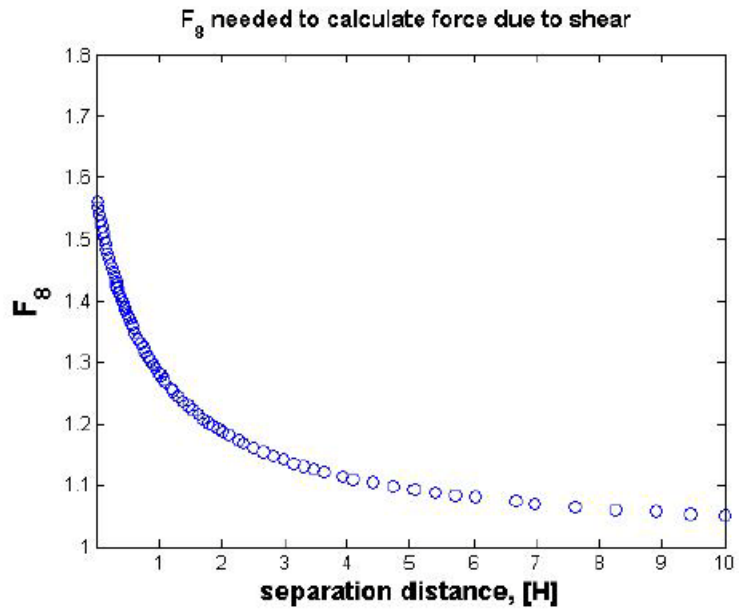

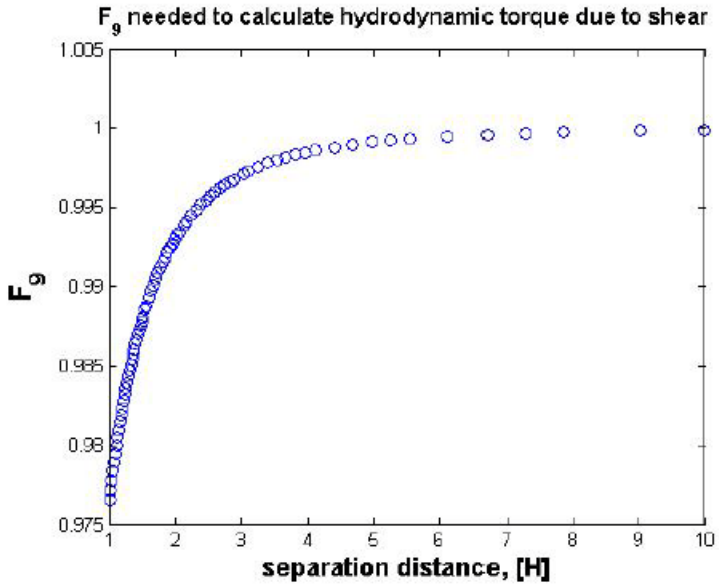

Figure 7. The figure shows that both F8 and F9 tend to one with increasing H. Source: work by dr. A. Raoof, Utrecht University (2016).

For H → 0, F8 and F9 approach the limiting values:

(45)

$$F_8 = 1.701$$

$$F_9 = 0.944$$

The trajectory equations can be expressed in the particle's local coordinate system:

(46)

$$U_{x'} = \frac{dx'}{dt} = \frac{F'_4}{6\pi\eta a} F_{x'} + G_{sh_x} z' F_3$$

$$U_{y'} = \frac{dy'}{dt} = \frac{F'_4}{6\pi\eta a} F_{'} + y G_{sh_y} z' F_3$$

$$U_{z'} = \frac{dz'}{dt} = \frac{F_1}{6\pi\eta a} F_{z'}$$

In this case F3 is the universal correction function for the parallel motion of a spherical particle in simple shear flow. F3 is approximated by the following equation:

(47)

$$F_3(H) \cong \frac{1}{0.754 - 0.256\ln(H)} \; for\; H < 0.15$$

$$F_3(H) \cong 1 - \frac{0.304}{(1+H)^3} \; for\; H > 0.15$$

Brownian Diffusion

By incorporating the Brownian force, the force balance equations can be extended. Brownian force has the character of white noise and is exerted on particles by the thermal motion of the medium size suspended molecules. Einstein's method is used to derive the expression of the diffusion matrix for particles of arbitrary shape.

The Brownian diffusion force has two properties:

(48)

$$\langle F_B \rangle = 0$$

$$\overline{F_B(t) F_B(t+\Delta t)} = 2kT\bar{\bar{R}}\delta_D(t) = 2kT\overline{\overline{M^{-1}}}\delta_D(t)$$

Where Sdt is the Dirac delta function.

The anisotropy of the translational diffusion coefficient occurs for particle motion near interfaces. The mean square displacements for diffusive motion of the particle in three dimensional space are:

(49)

$$\langle x^{*2} \rangle = 2D_{11}t$$

$$\langle y^{*2} \rangle = 2D_{22}t$$

$$\langle z^{*2} \rangle = 2D_{33}t$$

The translational diffusion tensor of a spherical particle near interfaces can be expressed as:

(50)

$$D = kT\bar{\bar{M}} = \begin{bmatrix} D_{||} & 0 & 0 \\ 0 & D_{||} & 0 \\ 0 & 0 & D_{\perp} \end{bmatrix} = D \begin{bmatrix} F_4'(H) & 0 & 0 \\ 0 & F_4'(H) & 0 \\ 0 & 0 & F_1(H) \end{bmatrix} I$$

Where D, D are the diffusion coefficients for perpendicular and parallel particle motion given explicitly by:

(51)

$$D_{||} = \frac{kT}{6\pi\eta a} F_4'(H)$$

$$D_{\perp} = \frac{kT}{6\pi\eta a} F_1'(H)$$

In this equation F1(H) and F4(H) are the universal correction functions which are defined before. These equations state that the mobility of the particle depends on the dimensionless distance from the interface.

The mean square displacement is given by:

(52)

$$\langle r^{*2} \rangle = 2D_{\perp}t + 4D_{||}t$$

In the above equation, D and D is substituted so the following equation is formed:

(53)

$$\langle r^{*2} \rangle = 2t \frac{kT}{6\pi\eta a} F_1(H) + 4t \frac{kT}{6\pi\eta a} F_4'(H)$$

However, in this case it should be noted that because the diffusion coefficients depend upon separation distance from the interface, the mean square displacement remains a well-defined quantity in a local sense only. In other words, it remains valid when the displacement remains much smaller than the particle distance from the interface.

Displacement vector:

Using equation 34 and adding an extra term for diffusion force:

(54)

$$\bar{U} = \frac{d\bar{x}}{dt} = \bar{\bar{M}}.\bar{F} + \bar{\bar{M}}_c.\bar{T}_0 + M.\bar{F}^B$$

By approximating U=dx/dt, where x is the spatial coordinate vector, this results in:

(55)

$$\Delta\bar{x} = \bar{\bar{M}}.\bar{F}\Delta\bar{t} + \bar{\bar{M}}.\bar{T}_0\Delta\bar{t} + \Delta\overline{X_B} + kT(\nabla.\bar{\bar{M}})\Delta t$$

The two latter terms belong to the Brownian motion component. The first term explains the Brownian motion random walk and the second term is for the gradient of the mobility matrix. The gradient of the mobility matrix is a vector and gives extra force towards the centre of the tube.

The Brownian motion random walk can be expressed as:

(56)

$$\Delta\overline{X_B} = \sqrt{2kT\Delta t\bar{\bar{M}}}.\bar{\varphi}$$

Where p is a random vector with a mean of zero, and will act independently of different particles and different time steps.

Note:

In a system at an equilibrium state, where only diffusion force is acting:

(57)

$$\nabla.\bar{J_B} = 0$$

Where Jb is the diffusive flux, which can also be defined as:

(58)

$$\bar{J_d} = -\bar{\bar{D}}.\nabla n$$

Where n is the number of concentration of particles.

If D is a matrix with spatially variating components (for example, due to the presence of the pore wall) then we will have:

(59)

$$\nabla.(D.\nabla n) = 0$$

This can be written in two terms as:

(60)

$$\left(\nabla.\bar{\bar{D}}\right)\nabla n + \bar{\bar{D}}\nabla^2 n = 0$$

The term $\nabla.\bar{\bar{D}}$ can be written as kt(dM).

Simple validity analysis:

For a simple case of a non-Brownian spherical particle in an infinite domain with no shear, Stokes drag force is active:

(61)

$$F_d = 6\pi\eta a U$$

So:

(62)

$$U = \frac{1}{6\pi\eta a} F_D$$

Equation (45) gives velocity for the x' direction:

(63)

$$U_{x'} = \frac{dx'}{dt} = \frac{F'_4}{6\pi\eta a} F_{x'} + G_{sh_x} z' F_3$$

Since there is no shear, G=0, so:

(64)

$$U_{x'} = \frac{F'_4}{6\pi\eta a} F_{x'}$$

Where Fx=Fd

As H increases F4 gets closer and closer to one (Fig. 8).

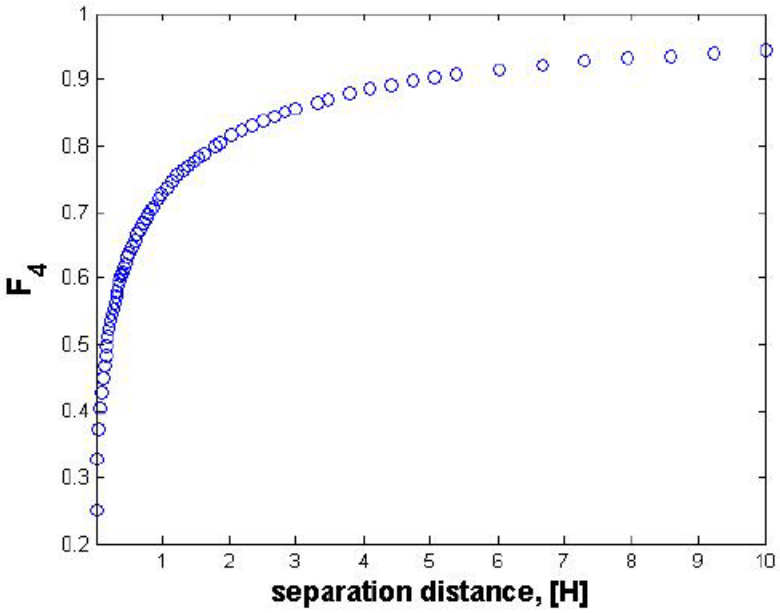

Figure 8. The figure shows that F4 increases and approaches 1 with increasing H. Source: work by dr. A. Raoof, Utrecht University (2016).

As H increases:

$$H \to \infty \quad \Rightarrow \quad \begin{cases} F_4 \to 1 \\ F_6 \to 1 \\ F_7 \to \infty \end{cases}$$

This means that F4 will be equal to one and:

(65)

$$U_{x'} = \frac{1}{6\pi\eta a} F_{x'}$$

Which is equal to equation (62).

3. Methods

As mentioned in the introduction, the effect of applied hydrodynamic on the colloid transport will be studied in this chapter. In section 3.1 a short summary of the model is given. In section 3.2 a schematic of the script used to calculate the velocity is shown. In section 3.3 a short summery of the main model is given. In 3.4 a schematic overview and specifics of the models are explained. Finally, in section 3.5 will be explained how certain variables are changed to answer the research question.

3.1 The model

The foundations of the model were laid by dr. Amir Raoof of Utrecht University, I have modified and added to his work. The model makes use of trajectory analysis method to view and model individual particles. This makes behaviour of particles in different situations easily observable. The first step was to make a script which modelled the stream flow within the pore. After this was finished and added to the main model further modifications were made and implemented to make the model run correctly.

3.2 Model Velocity Components Calculation Flowchart

On the next page a flowchart (Fig. 9) is presented of the script which calculates the velocity field within the constricted tube. The full script can be found in the appendix.

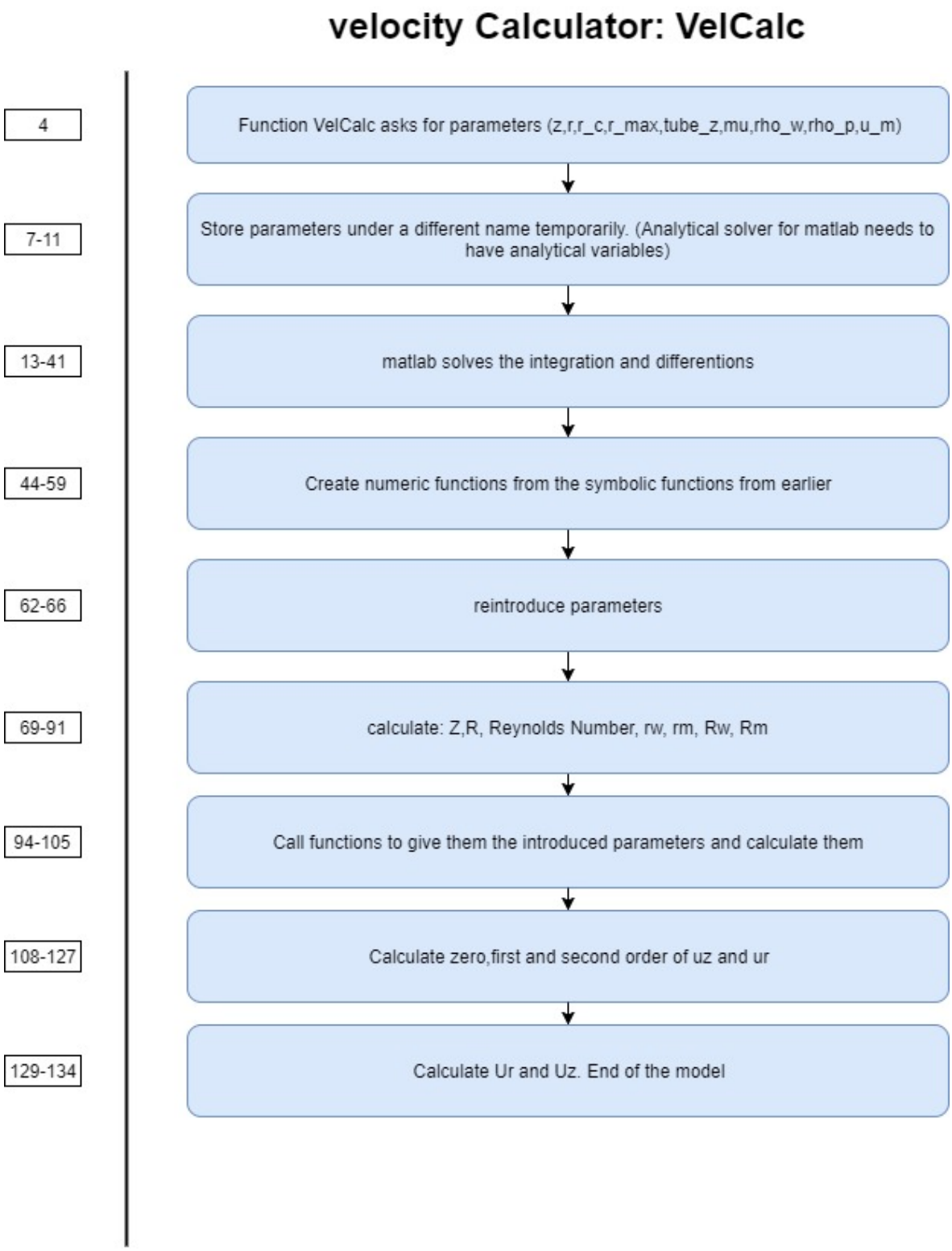

Figure 9. Flowchart velocity field script.

3.3 The main model

The main model works by first generating the pore shape geometry, which is parabolic. The model works by assuming that all forces which affect particle motion: hydrodynamic, electrokinetic and gravity, are additive and thus a mobility matrix can be made to calculate final particle velocity. As such that per timestep the resulting movement of the particle can be calculated. When the particle is away from the surface of the wall the particles will be predominantly be under influence of the velocity field, with slight changes made due to Brownian motion. However, the most interesting part is when the particle gets close to the wall and is subject to electrokinetic forces as well. When this happens the distance normal to the surface of the wall is taken and from there the acting forces on particle are calculated, this then gives the resulting movement due to shear or whether the particle aggregates. The model run ends when all particles have exited the constricted tube by either aggregating on to the collector surface or reaching the bottom of the tube.

3.4 Schematic overview and specifics of the model

On the next page is a schematic of the model used to calculate particle trajectory (Fig. 10). The model calculates the dimensionless distance to the wall by taking the cosine of arctangent of the particle, in degrees. This distance is then measured minus the radius of the particle, so you get the distance of the surface wall to the particle wall. Then this distance is divided by the particle radius, such that it is expressed in dimensionless distance of the particle radius.

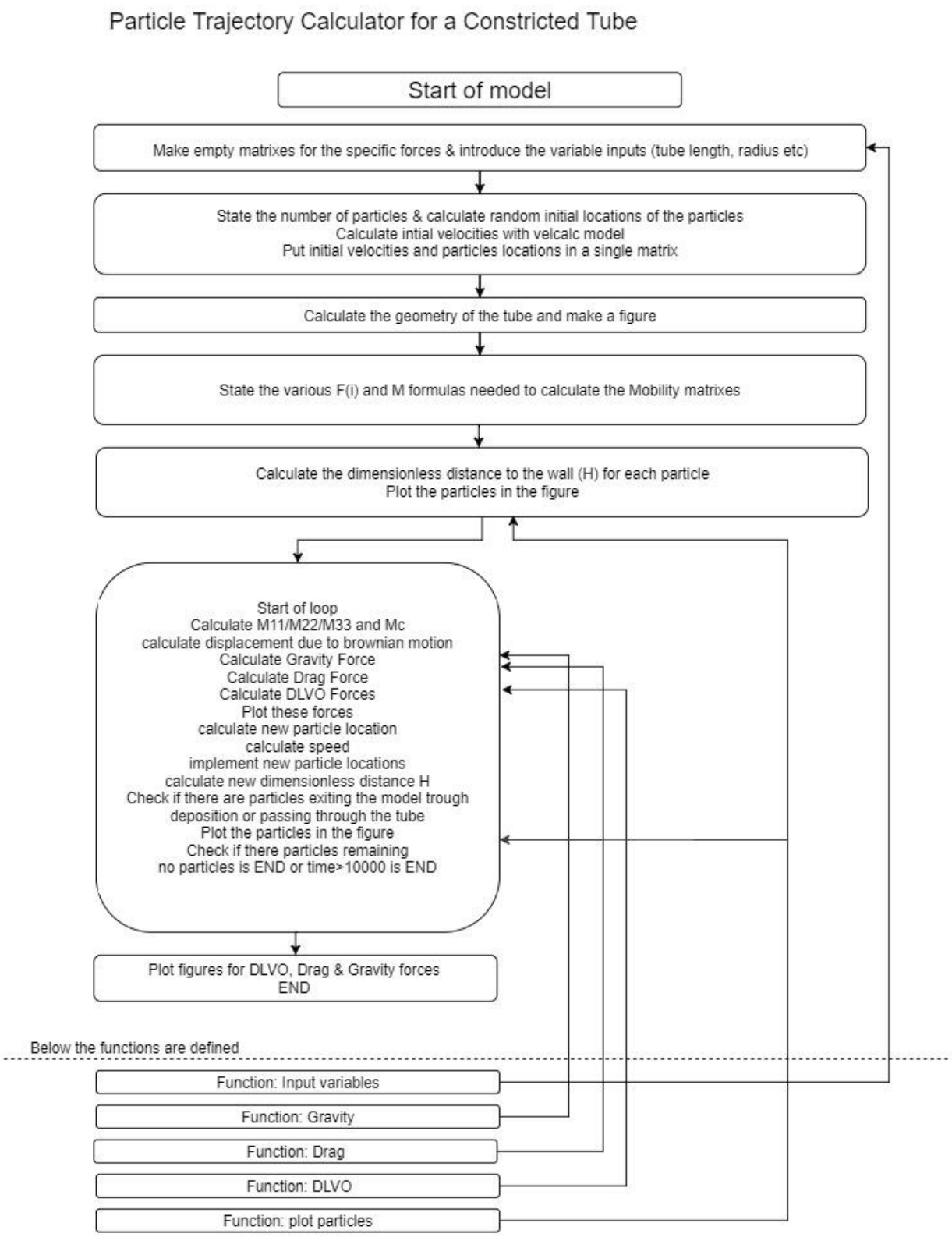

Figure 10. Schematic overview of the model.

3.5 How to answer the research question

The research question is:

"How is colloid attachment and detachment in a single pore affected by pore shape and velocity?"

To answer this question, the model is run with different values for pore shape and velocity, while the colloid attachment rate is measured. The existing hypothesis is that if velocity is increased the deposition rate will decrease, whether that may be due to the small radius of the constriction or due to a direct increase of velocity. The actual qualification and quantification of how the colloid detachment/attachment behaves is the subject of this study. To achieve this, the data from the different model runs is grouped together and a plotted together for colloid attachment vs constriction radius and colloid attachment vs velocity.

First part of the research

In the first part of the research a qualitative comparison is made between colloid attachment and detachment in a single pore versus both a changed velocity and a changed pore shape.

In table 1 is shown which parameters are used in the model.

Parameter	Value
N	10
Velocity	low (0.3e-6 m/s) to average (1.5e-6 m/s) to high (3e-6 m/s).
Construction radius	small (0.02e-3 m), average (0.15e-3 m) and straight (0.3e-3 m)
Radius at top	0.3e-3 m
Length tube	0.7e-3 m
DLVO force	+/- 40

Table 1. Parameters used. Loosely based on Chang et al. (2003).

The model was run with only two changed parameters: the constriction radius and the velocity through the chokepoint (μ). There are a total of nine runs: 3 for each minimum, maximum and average parameter. The speed is changed from low (0.3e-6 m/s) to average (1.5e-6 m/s) to high (3e-6 m/s). Each speed is run with three constriction radii: small (0.02e-3 m), average (0.15e-3 m) and straight (0.3e-3 m). This shows a clear picture of how the model behaves under various conditions. The particles are plotted in a straight line from

the centre point (at 0 m) to the wall (at 0.3e-3 m). There are 10 particles. The DLVO-force is kept at a constant maximum level because otherwise the particles wont properly aggregate unto the surface. The length of the tube is kept constant as well and is 0.7e-3 m. The DLVO forces are kept at a constant -40 and 40, this results in a barrierless energy curve.

Second part of the research

In this part a comparison is made between increasing velocities and colloid retention. The goal is to establish a more quantitative measurement of the effect of hydrodynamics on colloid retention under a same shape geometry.

Parameter	Value
N	10
Velocity	High to really high (3e-6 m/s, 6e-6 m/s, 12e-6 m, 30e-6 m/s, 60e-6m/s and 120e-6 m/s)
Construction radius	0.1e-3 m
Radius at top	0.3e-3 m
Length tube	0.7e-3 m
DLVO force	+/- 40

Table 2. Parameters used. Loosely based on Chang et al. (2003)

4. Results

In this chapter the results are shown from a series of model runs under changed conditions, as described in the methods. The results are divided in part 1 and part 2.

4.1 Model results part 1

The results of the first run of the model are shown in Figure 11, and show to the left drag, DLVO & combined forces acting on all particles. To the right is the modelled tube with the coloured particles represented within.

- *First run: High speed and small radius (μ =3^{e}-6 m/s, rc= 0.02^{e}-3 m)*

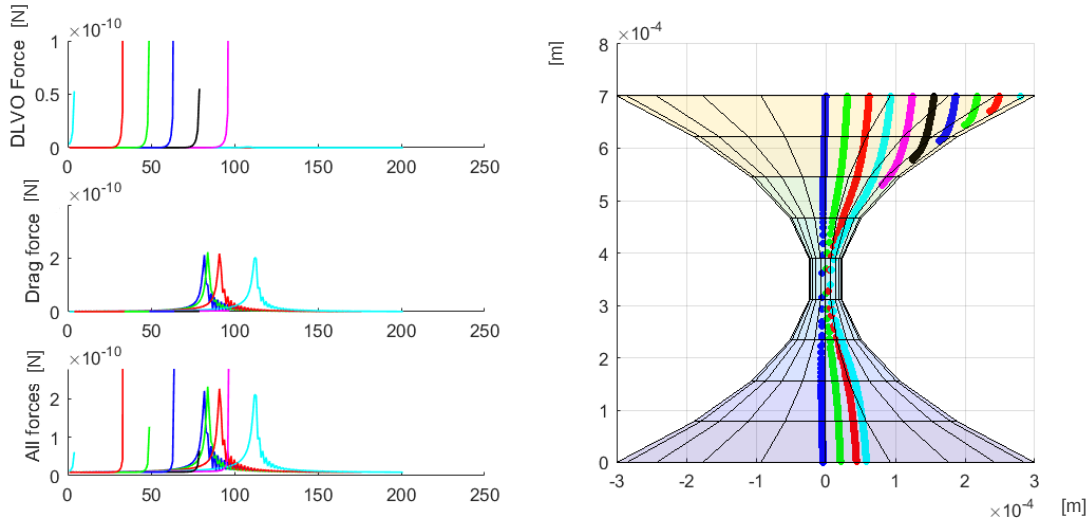

Figure 11. **High speed and small radius (*μ* =3^{e}-6 m/s, rc= 0.02^{e}-3 m)**

The DLVO force graph shows a very high peak for the red particle and some very tiny peaks for the other adsorbed particles. The drag force graph shows four very high peaks for the four particles which made it through the narrow constriction. The rest of the drag force figure shows horizontal lines because of the relatively low velocities when compared to the velocity through the constriction. The approximately smooth slope on the left side is in stark contrast to the other rocky side. This is because the particles reach such a velocity that they are propelled through the constriction into the lower speed zones on the other side, resulting in a high difference between said velocities and cause the model to slowly reach equilibrium again. Particle adsorption is at 60%.

- *Second run: High speed and average radius (μ =3^{e}-6 m/s,rc=0.15^{e}-3 nm)*

Below (Fig. 12) the results of the third run of the model are shown.

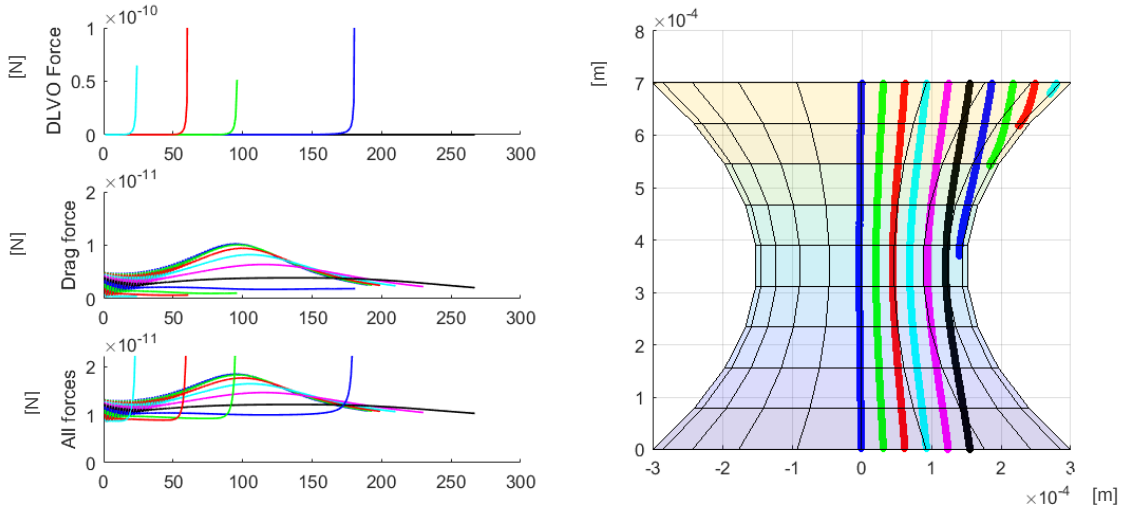

Figure 12. **High speed and average radius (*μ* =3^{e}-6 m/s,rc=0.15^{e}-3 nm).**

The DLVO force graph shows which particles adsorbed to the wall, which amounts to four. The drag force graph shows a much more smooth figure than in the previous two figures. This is because the constriction is not as narrow as it could be which makes for less of a difference in velocity. This is also means equilibrium is reached earlier and there is no need to reacquire equilibrium after passing through the constriction because the velocity isn't as high. Particle adsorption is at 40%.

- *Third run: High speed and large radius (μ =3^{e}-6 m/s,rc=0.3^{e}-3 nm)*

Below (Fig. 13) the results of the second run of the model are shown.

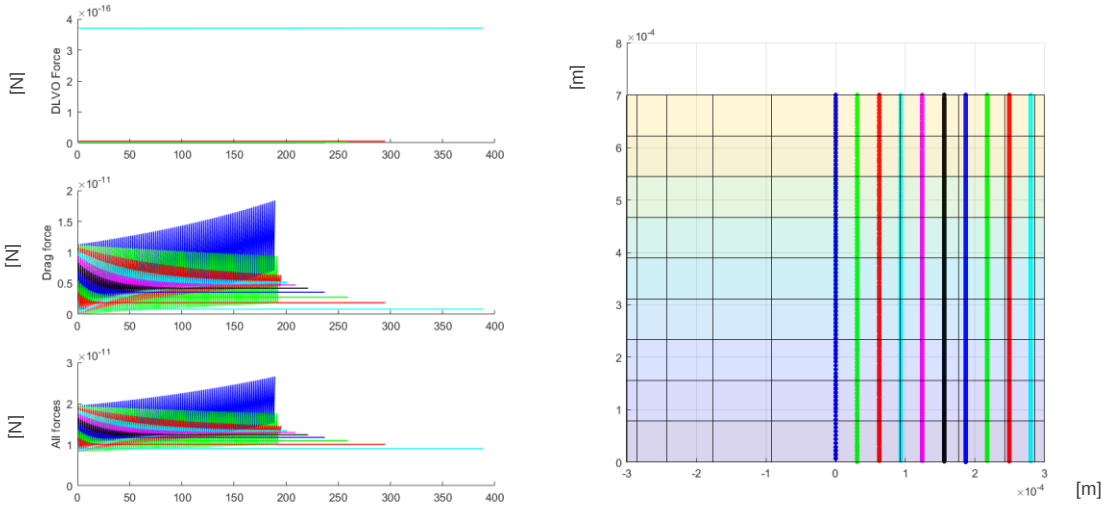

Figure 13. **High speed and large radius (μ =3^{e}-6 m/s,rc=0.3^{e}-3 nm).**

The velocity is the same as in the first run but this time there is no constricted area. This causes remarkable changes in drag force. Visible in the drag force figure is the slow reaching of equilibria for all particles but blue. The slowest velocities are measured at the wall of the cylinder and the highest are measured in the centre. Due to the straight wall no particle can come close enough to adsorb.

- *Fourth run: Low speed and small radius (*μ *=0.3^{e}-6 m/s,rc=0.02^{e}-3 nm)*

Below (Fig. 14) the results of the fourth run of the model are shown.

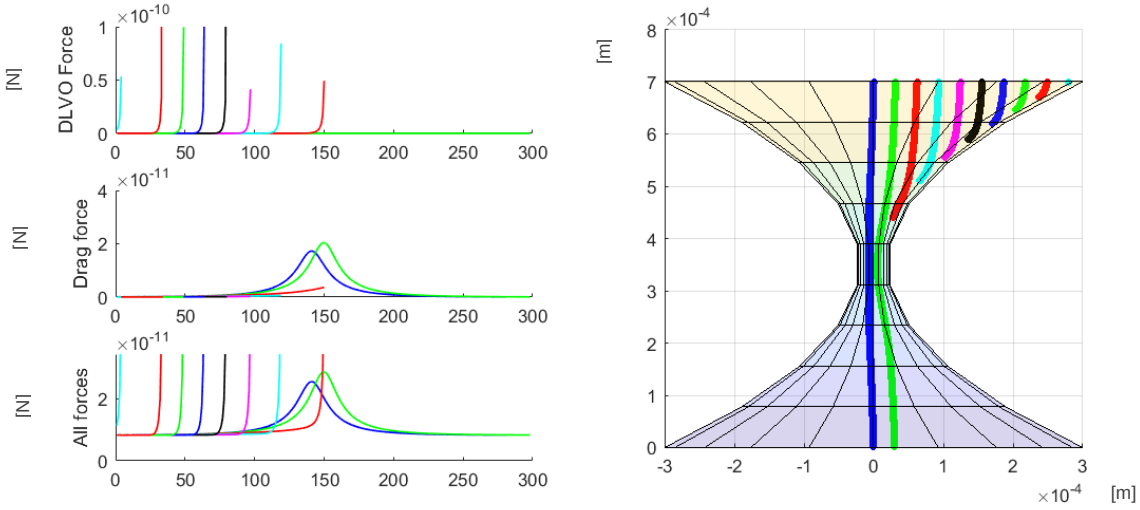

Figure 14. Low speed and small radius (μ =0.3e-6 m/s,rc=0.02e-3 nm).

In these set of runs (four to six) the velocity has been drastically lowered by an order of magnitude, from 3e-6 m/s to 0.3e-6m/s. This is visible as the maximum drag force is only about 2e-11 versus the 2e-10 maximum drag force in the first scenario. Only two particles made it through the constricted area and the rest have adsorbed to the wall. The particle trajectories are continuous and not dotted as seen in the first scenario. Particle adsorption is at 80%.

- *Fifth run: Low speed and average radius (*μ *=0.3^{e}-6 m/s,rc=0.15^{e}-3 nm)*

Below (Fig. 15) the results of the fifth run of the model are shown.

The drag force graph in this scenario is more elongated and with less of a peak than the second scenario has, due to the lower velocity. The particle trajectories are also less curving than in the second scenario. The second blue particle from the centre is also not as far down the tube as in scenario two. The particle adsorption is 40%.

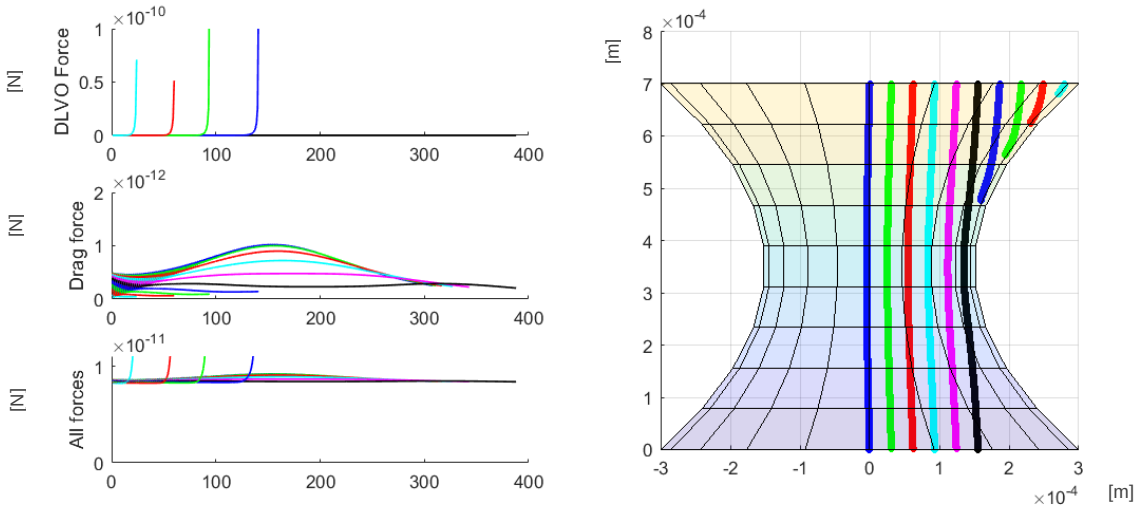

Figure 15. Low speed and average radius (μ =0.3^{e}-6 m/s,rc=0.15^{e}-3 nm)

- *Sixth run: Low speed and large radius (μ =0.3^{e}-6 m/s,rc=0.3^{e}-3 nm)*

Below (Fig. 16) the results of the sixth run of the model are shown.

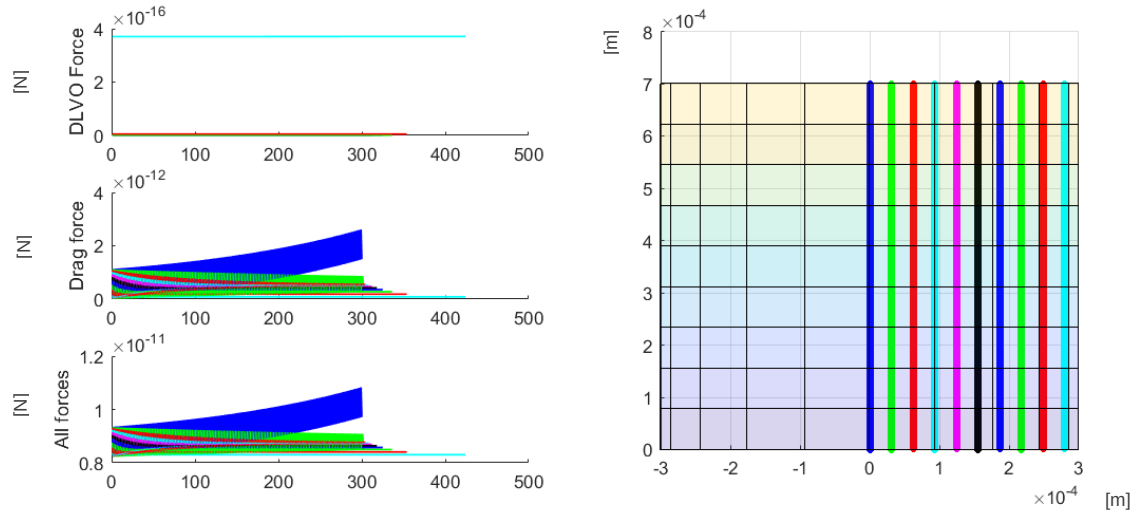

Figure 16. Low speed and large radius (μ =0.3e-6 m/s,rc=0.3e-3 nm)

The sixth scenario features a slow speed and straight cylinder geometry, equal to the third scenario. This time there is a bigger divergence between the drag force of the centre particle (blue) and the particle next to the centre (green). Also it seems like the blue particle has an increasing drag force and is closer to reaching equilibrium than in the third scenario.

- *Seventh run: Average speed and small radius (μ =1.5^{e}-6 m/s,rc 0.02^{e}-3 nm)*

Below (Fig. 17) the results of the seventh run of the model are shown.

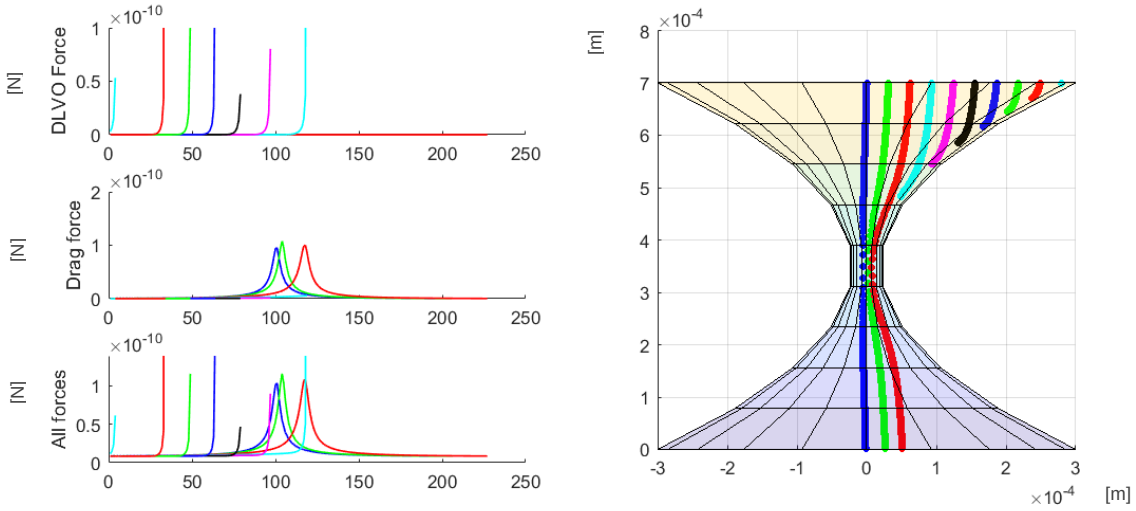

Figure 17. Average speed and small radius (μ =1.5 e-6 m/s,rc 0.02e-3 nm).

In the scenarios of seven, eight and nine the speed is of an average value, right in between the fastest and the slowest velocities. The maximum drag force reached is around 1e-10, whereas the highest drag force in scenario one is around 2e-10. In this scenario Particle adsorption is at 70%.

- *Eight run: Average speed and average radius (μ =1.5 ^{e}-6 m/s,rc=0.15^{e}-3 nm)*

Below (Fig. 18) the results of the eight run of the model are shown.

This scenario falls right between the second and the fifth. The particle trajectories are a bit more curved than in scenario five but not as curving as in scenario two. Particle adsorption is 40%.

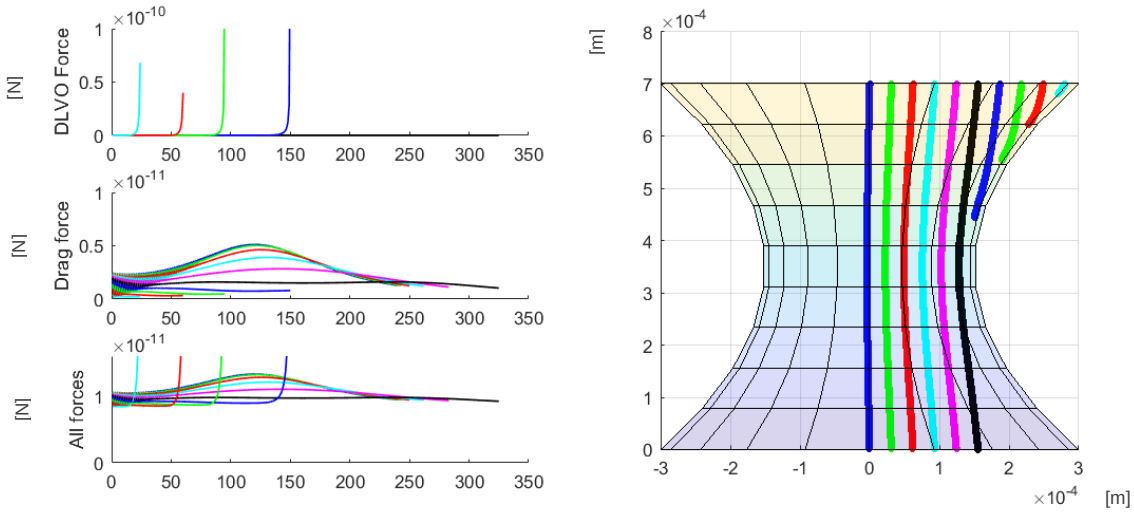

Figure 18. Average speed and average radius (μ =1.5e-6 m/s,rc=0.15e-3 nm).

- *Ninth run: Average speed and large radius (μ =1.5^{e}-6 m/s,rc=3^{e}-3 nm)*

Below (Fig. 19) the results of the ninth run of the model are shown.

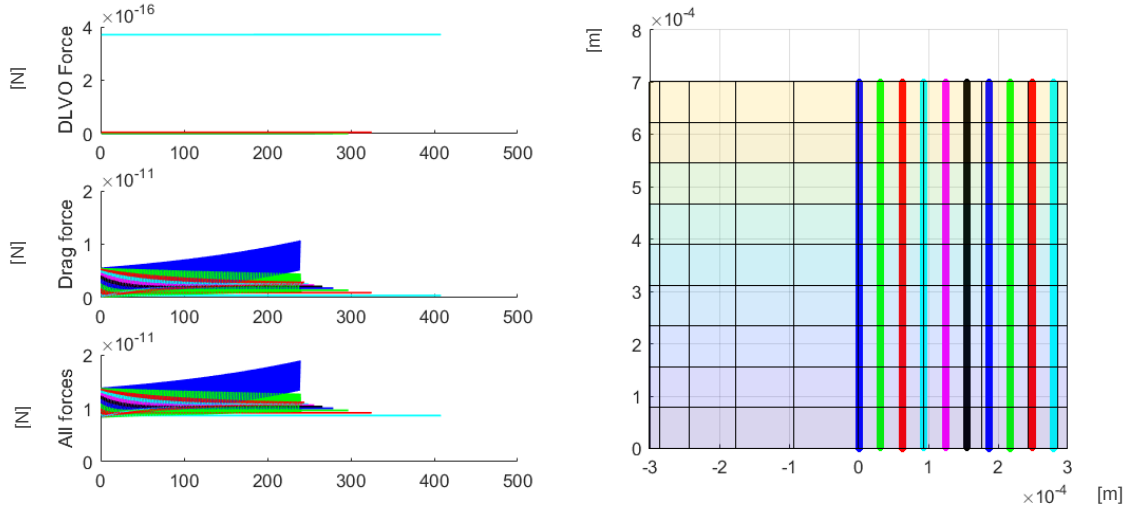

Figure 19. Average speed and large radius (μ =1.5e-6 m/s,rc=3e-3 nm).

This scenario is the average between the third and the sixth scenario. There is not as much difference between the centre (blue) and the next to centre (green) particles as seen in scenario six.

4.2 Results part 2

In this section a comparison is made between increasing velocities and colloid retention.

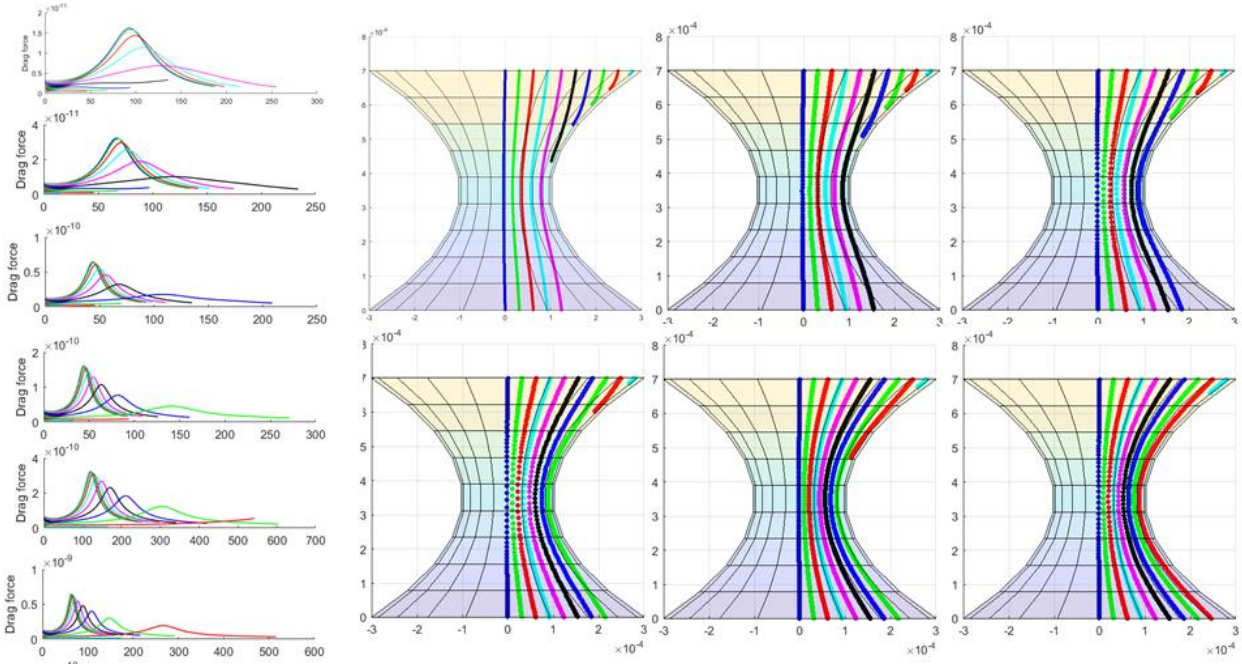

Figure 20. On the left are the drag force graphs from lowest speed on top to highest speed on the bottom. From the top left figure is the lowest speed to the highest speed on the bottom right. Forces are in newton and the graph is in [m] meters.

In the figure above (Fig. 20) there are various simulations visible under the same circumstance except for an increase in mu. The simulations are run with top left to top right: 3e-6 m/s, 6e-6 m/s, 12e-6 m/s and bottom left to bottom right: 30e-6 m/s, 60e-6m/s and 120e-6 m/s.

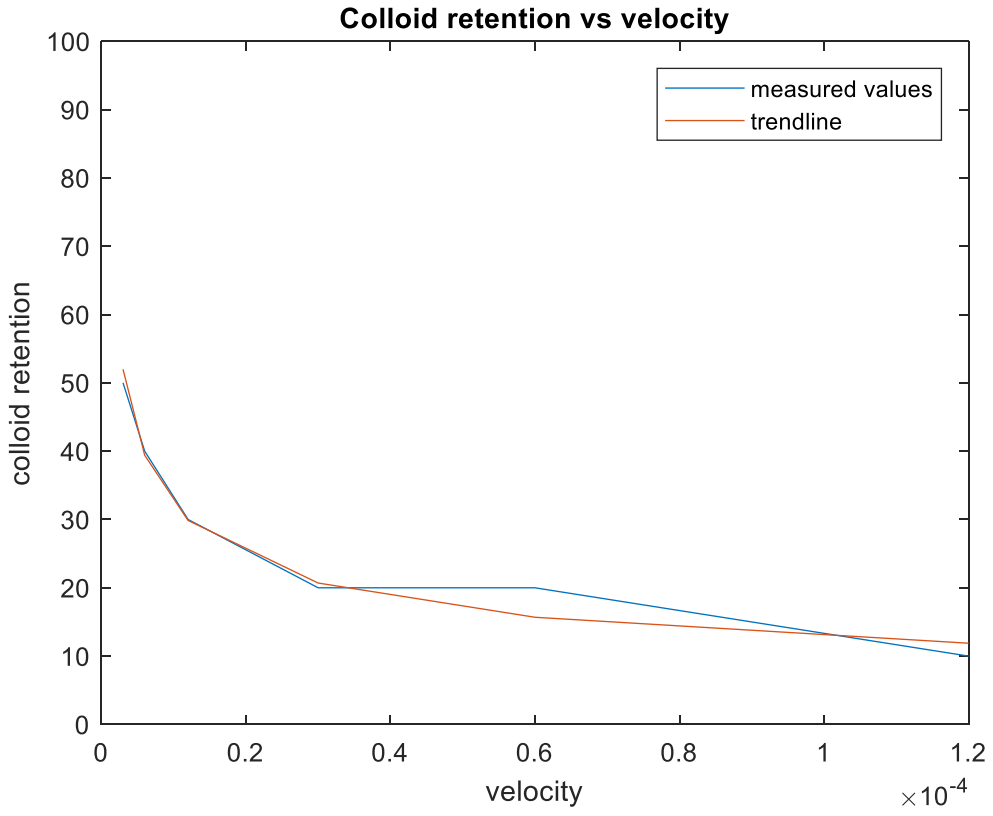

Figure 21. Plot of the colloid retention vs velocity. The formula for the trendline is Y=0.3212X^-0.4 with an R^2 value of 0.9451.

In figure 21 the colloid retention of the six previous runs is shown with an added trendline. The graph has not a linear shape. The decrease in colloid retention is the greatest for the three points, afterwards it starts to require bigger increase in velocity for the same effect. The formula for the trendline is y=0.3212x^-0.4. This means that the colloid retention is 0.3212*velocity^-0.4.

The base speed of 3e-6 m/s corresponds to about 0.25 meters travelled per day and the maximum speed of 120 m/s is around 10 meters per day which is still possible but very high for groundwater velocities. Reynolds number still remains very low due to the relatively low speed of groundwater flow and small diameter of the pore space, thus ensuring laminar flow.

5. Discussion

As mentioned in the introduction, previous research has indicated that the applied hydrodynamics can play a significant role in colloid retention in several natural environments (Torkzaban, Bradford, & Walker, 2007). By examining the results, we are led to the conclusion that applied hydrodynamics does indeed have a significant effect on colloid retention.

Shown below are the results again of scenarios one, four and seven (Fig. 22).

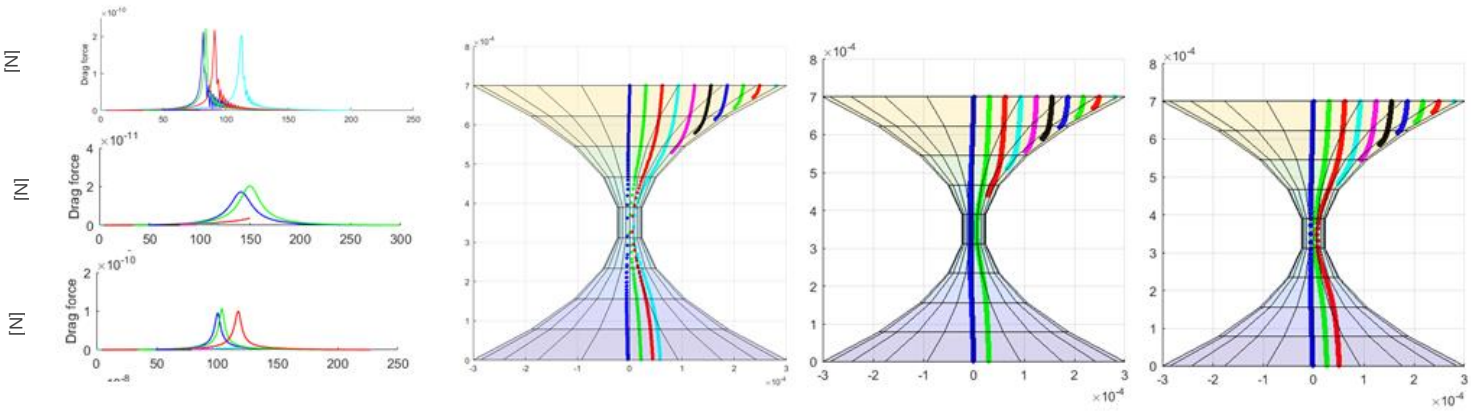

Figure 22. Results scenario 1, 4 and 7: small radius. Forces are in newton and the graph is in [m] meters.

The first, fourth and seventh scenarios show the most difference. Due to the narrow constriction the hydrodynamic force increases greatly, and this has great effect on colloid retention. The maximum drag force noted for the first scenario is at 2e-10 N whereas the maximum drag force for the second scenario is 0.1e-10 N. The adsorption rates (percentage of particles adsorbed) also vary from 60% to 80. This provides evidence that pore shape geometry greatly affects hydrodynamics, with increasing effect at narrow pore constrictions.

Shown below are the results of scenarios two, five and eight (Fig. 23).

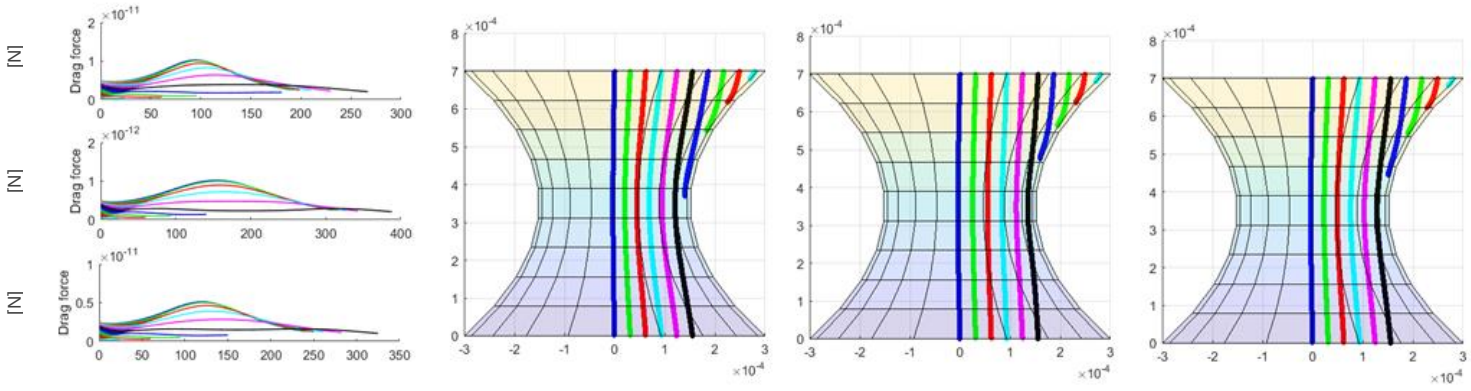

Figure 23. Results scenario 2, 5 and 8: average radius. Forces are in newton and the graph is in [m] meters.

When comparing the second, fifth and eighth scenarios although the particle adsorption rate stays the same the last particle to adsorb shows an increasing distance travelled. This is another piece of evidence that indicates the decreasing adsorption rate with an increase in velocity. Although not as heavily influenced as seen in other scenarios, this could be due to the relatively wide constriction radius. The wide constriction radius gives less rise of velocity and thus less of an effect on colloid retention. The shape of the drag force curve is also remarkable, showing a peak with steeper slopes for the fastest velocity and more gentle slopes for the slowest velocity.

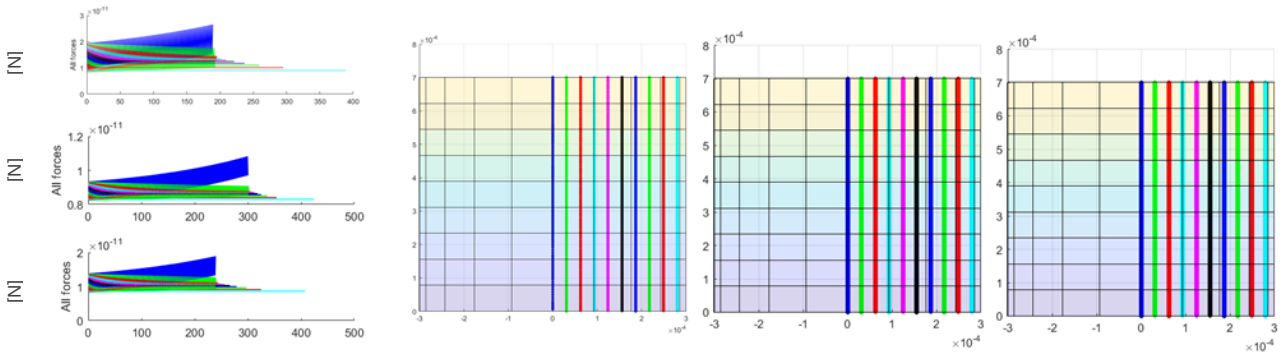

Figure 24. Results scenario 3, 6 and 9: large radius. Forces are in newton and the graph is in [m] meters.

When looking at the drag force graphs from scenarios three, six and nine (Fig. 24), it is not expected for the centre particle to keep increasing in speed. It should find an equilibrium value and stay at that value, and in this case it keeps increasing whereas there is no theoretical basis for an increase in velocity. The reason for blue not reaching equilibrium is because the drag force is calculated in such a way that the velocity field is compared to the actual velocity measured, for some reason the actual velocity is bigger than the velocity field causing a slight change where the result should be 0. This change results in an eventually increasing velocity. The particles to the side are influenced by the DLVO force and lose some

actual velocity so they eventually reach a state where the actual velocity is smaller than the velocity field and reach equilibrium.

Some limitations have to be addressed, the formulas used are an approximation of reality and the model is a simplification of reality resulting in a model which cannot be equal to reality even in the best scenario. There are also certain areas of the model which are still lacking in and of itself, for instance the increasing velocity in cylinder geometry.

Further research is necessary for an more in-depth understanding of the relationship between the different parameters. Increasing the quantity of runs with different parameters, which was unfortunately not possible for this project due to time constraints. It would be interesting to see how the model works when it is scaled up to a real-life measurement of small unit of pores and the results compared to real scenario.

6. Conclusion

The main research questions is:

"How is colloid attachment and detachment in a single pore affected by pore shape and velocity?"

As stated in the discussion I conclude that colloid attachment and detachment is indeed affected by pore shape geometry and applied hydrodynamics. With the most noticeable effects in narrow pore shaped constrictions and high velocities resulting in a higher rate of colloid retention. When the constriction radius was half of the maximum pore radius the effect of hydrodynamics on colloid retention changed substantially. There was no change in particle adsorption for all three scenarios although particles travelled a slightly longer distance before adsorbing, showing that even in this scenario high velocity retains its effect on particle adsorption- although on a substantially lower rate. In the straight cylinder scenarios there was no colloid retention. This leads to the conclusion that the effect of pore shape on colloid retention is strongest at very straight or very narrow pore shapes. During average constriction radii the effect of pore shape geometry and applied hydrodynamics on colloid retention was the lowest.

This study functions a testament to the importance of applied hydrodynamics on colloid retention. Utilizing the model and conclusions of this study to conduct further research will increase our understanding and have a potentially substantial impact on a wide spectrum of subjects, from medicine to water treatment (Torkzaban, Bradford, & Walker, 2007).

References

Boström, M., Deniz, V., Franks, G. V., & Ninham, B. W. (2006). Extended DLVO theory: Electrostatic and non-electrostatic forces in oxide suspensions. *Advances in Colloid and Interface Science*, *123–126*(SPEC. ISS.), 5–15. http://doi.org/10.1016/j.cis.2006.05.001

Brittanica Online Encyclopedia. (n.d.). Colloid. Retrieved June 21, 2017, from https://www.britannica.com/science/colloid

Chang, Y. I., Chen, S. C., & Lee, E. (2003). Prediction of Brownian particle deposition in porous media using the constricted tube model. *Journal of Colloid and Interface Science*, *266*(1), 48–59. http://doi.org/10.1016/S0021-9797(03)00636-2

Tien, C., & Ramarao, B. V. (2007). *Granular filtration of aerosols and hydrosols* (2nd ed.). Amsterdam: Elsevier.

Torkzaban, S., Bradford, S. A., & Walker, S. L. (2007). Resolving the coupled effects of hydrodynamics and DLVO forces on colloid attachment in porous media. *Langmuir*, *23*(19), 9652–9660. http://doi.org/10.1021/la700995e

TU Delft. (n.d.). Granular filtration. Retrieved June 21, 2017, from https://ocw.tudelft.nl/wp-content/uploads/Granular-filtration-1.pdf

Tufenkji, N., & Elimelech, M. (2005). Breakdown of colloid filtration theory: Role of the secondary energy minimum and surface charge heterogeneities. *Langmuir*, *21*(3), 841–852. http://doi.org/10.1021/la048102g

Yao, K.-M., Habibian, M., & O'Melia, C. (1971). Water and Waste Water Filtration: Concepts and Applications, *5*(11), 1105–1112.

Zeta-Meter, I. (1997). Zeta-Potential: A Complete Course in 5 Minutes. *Technial Note*, 1–8. Retrieved from http://scholar.google.com/scholar?hl=en&btnG=Search&q=intitle:Zeta+Potential+:+A+Complete+Course+in+5+Minutes#0%5Cnhttp://scholar.google.com/scholar?hl=en&btnG=Search&q=intitle:Zeta-Potential:+A+Complete+Course+in+5+Minutes#0

Appendix

Model:

9-12	logic variables control the plots
14-15	tic/clc
23	tubez rmax rc counter are made global
26-30	declareer info in partities (grav/diff/DLVO/sum)
31-35	declareer empty matrix for grav/diff/DLVO/SUM
40-41	Make fig. tube and put hold
42-53	give particle radius,tube length,dt,rmax etc & function inputs (which are added down below)
60	Give number of particles
75-84	give initial locations for N particles, in init R,Z and Theta (angular location)
87-88	make empty matrix for N for init_ur/uz
89-93	Calculate init_ur/uz
102-107	put the init locations r/z and velocities ur/uz per N particle in a matrix
115	give function for calculating wall geometry
118-129	plot the tube for z(0>z>1) and draw the geometry in fig. tube
134-149	calculate F1,F4,F6,F7,F8 kc_p and M11,M22,M33
151-164	plot these F functions if logic variable is 1
193	calculate H (dimensionless distance) by calc distance to wall for particle N – init location
195-199	Calculate H for every particle
201	Plot particles in fig. Tube
202-205	Start of loop for 1:N(particles)
215-230	for every particle N calculate M11,M22,M33
230-233	Calculate Mc, namely kc_p
234-237	Calculate displacement due to Brownian motion and vectorizer
238-240	Calculate Div of M
242-244	Calc Slope
248-251	Calc Gravity Force
253-259	Calc Drag Force
261-265	Calc DLVO force
267-277	tell matlab to print (say) forces in the command widow for added visibility
275-279	Insert the forces into the info matrix for informative overview
281-309	Plot Drag/dlvo/all forces
314-317	Calc displacement dx, convert to radial displacement dr(r-direction)/dg(z-direction)
321-322	Calculate velocity by dividing distance by time, dr/dt, dg/dt
325-337	Implement these new locations into the model
343	End loop for particle forces calculation
348-353	Calculate New H for the new location
356-371	Calculate if there are particles exiting (either through the side or through the bottom)
379-383	plot particles & check if there are particles remaining, if not END or if time>10000 END

437	End of particle displacement calculation, the model run ends only if all particles are deposited, either by passing through the wall or exiting the tube at the bottom
438-445	Plot figures DLVO, Drag, Grav in Fig 2
450-457	State func Input, these are just variables
461-466	Define function: Gravity, this forms the formulas which calc f_grav
469-504	Define function: Drag force
507-609	Define function: DLVO force
611-649	Define function: Plot particles

END OF MODEL